

Group Conductivity and Nonadiabatic Born Effective Charges of Disordered Metals, Warm Dense Matter, and Hot Dense Plasma

Vidushi Sharma^{1,2,3,*} and Alexander J. White^{1,†}

¹Theoretical Division, Los Alamos National Laboratory, Los Alamos, NM 87545, USA

²Center for Nonlinear Studies, Los Alamos National Laboratory, Los Alamos, NM 87545, USA

³Applied Materials and Sustainability Sciences, Princeton Plasma Physics Laboratory, Princeton, NJ 08540-6655, USA

(Dated: February 27, 2025)

The average ionization state is a critical parameter in plasma models for charged particle transport, equation of state, and optical response. The dynamical or nonadiabatic Born effective charge (NBEC), calculated via first principles time-dependent density functional theory, provides exact ionic partitioning of bulk electron response for both metallic and insulating materials. The NBEC can be transformed into a “group conductivity,” *i.e.*, the *electron* conductivity ascribed to a subset of ions. We show that for disordered metallic systems, such as warm dense matter (WDM) and hot dense plasma, the static limit of the NBEC is different from the average ionization states, but that the ionization state can be extracted from the group conductivity even in mixed systems. We demonstrate this approach using a set of archetypical examples, including cold and warm aluminium, low- and high- density WDM carbon, and a WDM carbon-beryllium-hydrogen mixture.

Warm dense matter (WDM) physics is key to many complex systems [1–3]. WDM is generated in the initial phases of an inertial confinement fusion experiment and forms the cores of planetary systems, ice giants and exoplanets [4–7]. Its theoretical description poses a challenge. Nearly every analytical model for materials properties in WDM or hot dense plasma (HDP) regimes involves the average ionization state, *i.e.*, the effective or partial charge of ions, Z_{eff} [8–11]. This includes electronic and thermal conductivity [12–16], electron-ion relaxation rates [17], X-ray scattering [18–21], charged particle stopping power [22–29], inverse Bremsstrahlung absorption [30–32], as well as equation of state [33–35], ionic transport properties [36, 37], and multi-species mixing rules [38–43].

In a weakly coupled plasma regime, where degeneracy and ion correlations are negligible, the Saha model can be applied [44, 45]. For highly degenerate plasmas, the Thomas-Fermi model can be utilized but it does not account for discrete electronic levels [44, 46]. When strong ion correlations emerge at liquid or solid densities, *ab initio* multi-atom quantum mechanical simulations are imperative for determining Z_{eff} . This is challenging because Z_{eff} is not a well-defined observable, *i.e.*, there is no unique quantum operator which defines it.

There exists a gamut of charge partitioning schemes frequently employed in quantum chemistry, such as Mulliken [47], Bader [48], Hirshfeld [49], etc [50]. However, in disordered metals and in the WDM regime, wherein a significant number of electrons behave as “nearly-free”, these assignments become substantially more difficult and arbitrary [51]. An alternative approach is to extract Z_{eff} from well-defined observables, *e.g.*, the electrical conductivity [52, 53] or the electronic density of states

[54, 55]. However, these are *bulk* properties of the system, not atomically resolved. This prevents the determination of Z_{eff} distributions, or in the case of multi-component mixtures, the values for different elements. In this letter, we show that by exploiting the nonadiabatic forces on atoms we can efficiently extract not only an element-specific average charge, \hat{Z}_{eff}^G , but also the fully atomistically resolved conductivity σ^G , and thus the macroscopic dielectric, reflectivity and absorption spectrum. This approach is generally applicable to models where the assignment of optical response to a subset of atoms is desired, *e.g.*, surface atoms, defects, and moieties, molecular functional groups, and alloys.

The static *Born* (or transverse [56]) effective charge tensor (BEC, \hat{Z}_a^*) is a well-defined quantum observable [57]. It is defined as the negative of the change in the atomic force vector (\mathbf{F}^a) with respect to an applied electric field vector (\mathbf{E}), or equivalently, the change in the electronic polarization vector (\mathbf{P}) with respect to an atomic displacement vector ($\delta\mathbf{R}^a$) shifted by the bare nuclear charge (Z_a) :

$$\hat{Z}_a^* = -\frac{\partial \mathbf{F}_a}{\partial \mathbf{E}} = Z_a \hat{I} + \frac{\partial \mathbf{P}}{\partial \mathbf{R}^a}, \quad (1)$$

where \hat{I} is the identity matrix, and ‘*a*’ indexes the atom. For gapped materials, *i.e.*, insulators and semiconductors, \hat{Z}^* can be calculated via perturbation theory [58]. However, for metallic systems and doped semiconductors, the electric polarization is ill-defined in the static limit [59], and the static BEC has often been assumed to be ill-defined as well [60]. Recently, Dreyer, Coh, and Stengel (DCS) used the concept of *nonadiabatic* or *dynamical* BEC (NBEC, $\hat{Z}_a^*(\omega + i\gamma)$), to extend BEC to metals [61]. Here ω is the frequency of the perturbing field and γ is a small positive number. In the zero-frequency limit, $\omega \rightarrow 0$, the usual BEC is recovered [61].

The DCS sum rule states that the sum of all NBEC’s,

* vidushi@princeton.edu

† alwhite@lanl.gov

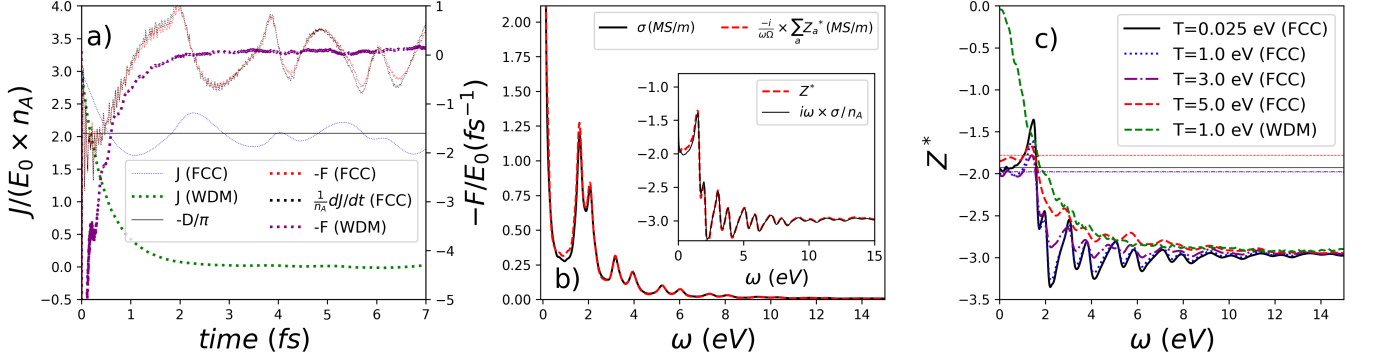


FIG. 1. Aluminium at solid-state density $\rho = 2.7 \text{ g/cm}^3$. a) fcc at $k_B T = 0.025 \text{ eV}$, disordered (WDM) at $k_B T = 1.0 \text{ eV}$, on the vertical axes: (left) J is scaled such that the signal is proportional to the number of electrons per atom, (right) negative of the force is scaled by E_0 yielding units of inverse time. Here, $-D/\pi$ is plotted for the fcc case. b) Current- and force-derived conductivity (Eq. (5)), and the conductivity- and force-derived average NBEC (inset, Eq. (3)) for fcc Al at $k_B T = 0.025 \text{ eV}$. c) NBEC for fcc geometry at $k_B T = \{0.025, 1.0, 3.0, 5.0\} \text{ eV}$, and disordered (WDM) phase at $k_B T = 1.0 \text{ eV}$.

divided by the cell volume Ω , yields the “Drude Weight”,

$$\frac{1}{\Omega} \sum_a \hat{Z}_a^*(0 + i\gamma)|_{\gamma \rightarrow 0} = -\frac{\hat{D}}{\pi}, \quad (2)$$

establishing a generalization of the acoustic sum rule applicable to both insulators ($\hat{D} = 0$) and metals ($\hat{D} \neq 0$) [62]. This Drude weight is the “truly-free” electron contribution to the electrical conductivity tensor ($\hat{\sigma}$). It is proportional to the number of electrons that, having “high inertia” or weak-coupling to the ion lattice, do not respond to a rigid translation of the ionic sublattice or equivalently, do not relax to their ground-state after being kicked by an instantaneous uniform electric field [63, 64]. However, due to electron relaxation in disordered systems $\hat{D} \rightarrow 0$, and thus $\sum_a \hat{Z}_a^*(\omega)|_{\omega \rightarrow 0} \rightarrow 0$ as well, even in gap-less electronically-conducting systems such as disordered metals or WDM. The average of the diagonal of the NBEC tensor, $\bar{Z}^*(\omega \rightarrow 0)$, cannot then be directly taken as a measure of Z_{eff} which must be finite for conductive systems. In these cases, electrons are only “nearly-free” rather than “truly-free” [65]. A finite scattering time must be taken into account when determining Z_{eff} from $\bar{Z}^*(\omega)$. As we will see, this can be done utilizing the finite frequency information available from nonadiabatic dynamics.

At finite frequency, the generalized DCS sum rule is written as,

$$\frac{1}{N_a} \sum_a Z_a^*(\omega) \equiv \bar{Z}^*(\omega) = i \frac{\omega}{n_a} \sigma(\omega) \equiv \bar{Z}_{\text{CD}}^*(\omega), \quad (3)$$

where N_a is the number of atoms and n_a is the atomic number density. We define $\bar{Z}_{\text{CD}}^*(\omega)$ as a conductivity-derived average (CDA-) NBEC. This is simply a consequence of the conservation of momentum [66–68]; the time-derivative of the total canonical electron momentum must oppose the total change in the atomic forces minus the contribution due to the bare ion interacting with the

electric field,

$$\sum_a \delta \mathbf{F}^a(t)|_{\mathbf{R}^a(t)=\mathbf{R}^a(0)} - Z_a \mathbf{E}(t) = -\Omega \frac{d}{dt} \mathbf{J}(t). \quad (4)$$

In this fixed-ion limit, we assert that the momentum transferred to a particular atom or group of atoms (*e.g.*, atoms of the same element) can be used to define a unique group (G) conductivity,

$$\sum_{a \in G} \frac{-i}{\Omega \omega} Z_a^*(\omega) \equiv \sigma^G(\omega), \quad (5)$$

$$\sum_G \sigma^G(\omega) \equiv \sigma^{FD}(\omega) = \sigma(\omega). \quad (6)$$

Upon summing over all groups the force-derived conductivity (σ^{FD}) is equivalent to the conductivity from the generalized DCS sum rule in Eq. (3). This transformation gives clear meaning to the real and imaginary parts of the NBEC at all frequencies, allowing for the extraction of atomistic details of the electron transport.

We calculate the NBEC and conductivity by simultaneously obtaining the time-dependent change in the atomic forces and current density in response to an instantaneous macroscopic external electric field pulse along the x -direction, $E_x(t) = \delta(t)E_{0,x}$. In this letter, we focus on isotropic systems; the diagonals of the NBEC and conductivity tensors are evaluated as,

$$Z_{xx}^a(\omega) + Z_a = \int dt e^{i\omega t - \frac{1}{4}\gamma^2 t^2} \Theta(t) \frac{F_x^a(t) - F_x^a(0)}{E_{0,x}}, \quad (7)$$

$$\sigma_{xx}(\omega) = \int dt e^{i\omega t - \frac{1}{4}\gamma^2 t^2} \Theta(t) \frac{J_x(t)}{E_{0,x}}. \quad (8)$$

While this approach to probe the linear-response conductivity has been previously reported [52, 69–71], the NBEC tensors have never been investigated in the WDM-HDP regime.

Our approach for calculating $\mathbf{F}^a(t)$ and $\mathbf{J}(t)$ is outlined in Supplemental Material Sec. S1 [52, 61, 63, 64, 72–81]. Recently, Wang *et al.* provided a phenomenological framework for computing the finite-frequency NBEC for crystalline systems, using Time-Dependent Density Functional Theory (TD-DFT), [82] by calculating the current response to an instantaneous atomic displacement in crystalline systems [75]. Formally equivalent to Eq. (7), this approach lacks computational efficiency, especially for multi-atom (disordered) systems. Our methodology allows for a simultaneous computation of $\sigma(\omega)$ and $Z_a^*(\omega)$ for all atoms from a single TD-DFT simulation. Notably, since we calculate only dynamical observables, any time-dependent electronic structure approach can be used. Without loss of information, from Eqs. (3) and (5), we consider and compare only the real parts of $\sigma(\omega)$, $\sigma^{FD}(\omega)$, $\bar{Z}^*(\omega)$ and $\bar{Z}_{CD}^*(\omega)$, *vide infra*.

Figure 1(a) shows the time-dependent current density (\mathbf{J}), and atomic forces (\mathbf{F}) in response to an instantaneous electric field pulse applied at $t = 0$ for the cases of room-temperature fcc aluminium ($k_B T = 0.025$ eV), and warm dense disordered aluminium ($k_B T = 1.0$ eV). A Drude weight of 2.04 (Eq. (2)) is extracted for fcc Al in good agreement with previous results [75], see Supplemental Material. From Eq. (4), $\frac{1}{n_a} \frac{\partial \mathbf{J}}{\partial t}$ is shown to be directly proportional to the average force; interestingly, unlike the fcc case $\mathbf{J}(t)$ in WDM decays to zero due to disorder.

In Fig. 1 (b) the conductivity calculated from the current density ($\sigma(\omega)$) is compared with the conductivity derived from the NBEC ($\sigma^G(\omega)$, Eq. (5) used in conjunction with Eq. (2)) for fcc Al. The Drude contribution is added as a Lorentzian centered at $\omega = 0$ with a tenth of the artificial broadening (*vide infra*, Supplemental Material S2). The true width of this peak depends on lattice vibrations and their coupling to the electrons, which we do not consider here. Similarly, the inset of Fig. 1(b) shows an agreement between $\bar{Z}^*(\omega)$ and $\bar{Z}_{CD}^*(\omega)$, Eq. (3). Finally, Fig. 1 (c) displays $\bar{Z}^*(\omega)$ computed for a range of electronic temperatures in the fcc Al structure along with disordered phase Al at $k_B T = 1.0$ eV. The electron transport properties in Al are largely unaffected by the increased electronic temperatures; the Drude weight remains ~ 2 for up to $k_B T = 5$ eV. Going from perfectly crystalline (blue-dotted) to disordered (green-dashed) eliminates the Drude contribution and $\bar{Z}^* \rightarrow 0$ in the static limit. This illustrates that Z_{eff} , which should be finite, and $\bar{Z}^*(\omega \rightarrow 0)$ are inherently different quantities in disordered systems.

We now propose the extraction of the average Z_{eff}^G from $\bar{Z}_G^*(\omega)$ in warm dense matter. As was used for the group conductivity, G indexes a given group of ions. We follow a typical approach of fitting the conductivity to a Drude model. However, we also need to account for static charge transfer between groups, $\Delta Z_{CT}^G \equiv \bar{Z}_G^*(0)$, and bound-free transitions. For group conductivity, the f-sum rule is now modified to include both the average

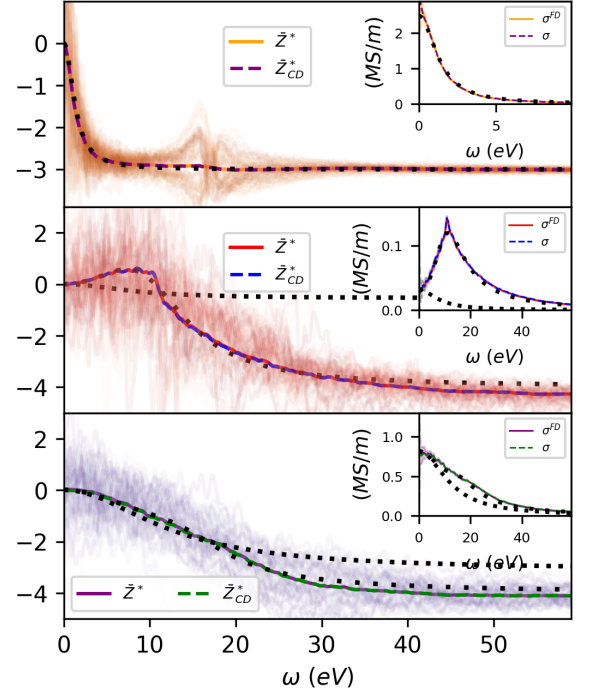


FIG. 2. The top panel shows the NBEC (inset- conductivity) for WDM disordered Al at $k_B T = 1.0$ eV, while the middle and lower panels show low-density (0.5 g/cm^3) and solid-density (3.5 g/cm^3) warm dense carbon systems at $k_B T = 1.0$ eV. The gradient-shaded lines show individual contribution of atoms to the spectra. (Dense/Sparse) dotted black lines are the (Drude-only/full) fits. Insets show ± 1 standard error of the force-derived conductivity as shaded bands.

bare-ion charge of the group, Z_G , and ΔZ_{CT}^G ,

$$\frac{2}{\pi} \int_0^\infty d\omega \sigma^G(\omega) = (Z_G + \Delta Z_{CT}^G) n_G, \quad (9)$$

where n_G is the number density of ions in group G . This follows from a straightforward application of the Kramers-Kronig relations to the force response. We use a modified Drude-Lorentz model, Supplemental Material Sec. S4, to fit the $\sigma^G(\omega)$ and extract Z_G . If G includes all atoms of the system then $\Delta Z_{CT}^G = 0$. Drude-like behavior is inherently classical and emerges from quantum systems only when considering many ions. We identify that this approach is not applicable when G includes too few atoms. Therefore working in the large system size limit for mixed systems, we fit the conductivity for G comprising all atoms of a given elemental species.

In Fig. 2 we show the average NBEC spectrum, $\bar{Z}^*(\omega)$ (solid and dashed lines), along with individual atom contributions (gradient-shaded), and (insets) $\sigma^G(\omega)$ for WDM systems. These average force-derived quantities are equivalent to their counterparts calculated from the current density, see Supplemental Material S3. While $\bar{Z}^*(\omega)$ for Al is an essentially featureless-dissipative spectrum; the individual $Z^*(\omega)$ show transition peaks be-

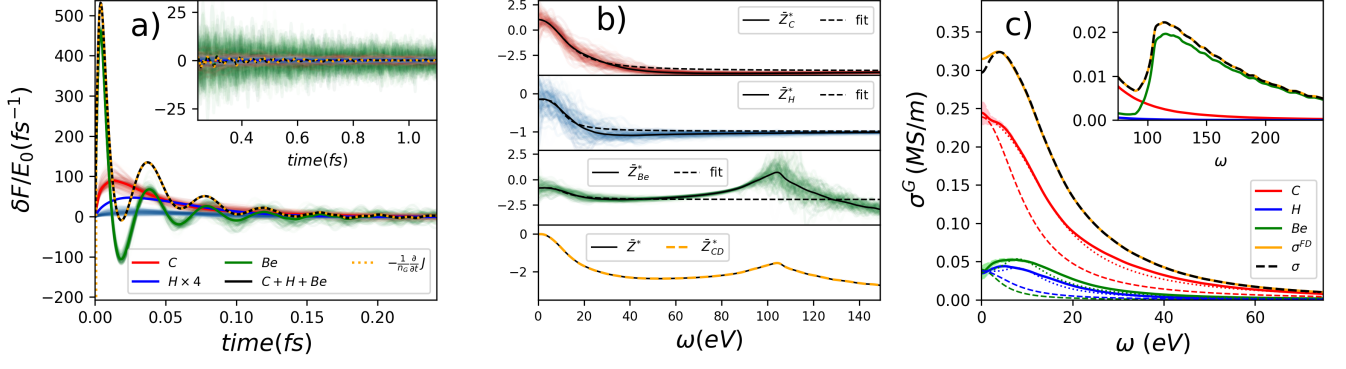


FIG. 3. Carbon Hydrogen Beryllium mixture, 1.37 g/cm^3 , $k_B T = 5 \text{ eV}$. *a*) The time-dependent individual and element average forces, $F_x(t) - F_x(0)$, sum of the averages (black), and $3 \times$ scaled time-derivative of the current-density per atom (orange). *b*) NBE for different elements with average and modified Drude-Lorentz fit, bottom-average of all NBE (black) and CDA-NBE (orange). *c*) The total FD conductivity, along with the components from each element. The inset of *a* (resp. *c*) extends the time (resp. frequency) domain.

tween $\hbar\omega = 10$ to 20 eV which average to zero, indicating no net momentum transfer from the electrons. These occur near the forbidden $\text{Al}^{2+} 3s$ to $3d$ or $4d$ transitions [83].

Here, $\sigma(\omega)$ or $\sigma^{FD}(\omega)$ fit readily to a Drude model yielding $Z_{\text{eff}} = 3.0$ with a scattering time, $\tau = 0.48 \text{ fs}$. To make contact with the plasma physics models, we compare with the average-atom DFT code **Tartarus** [84] which furnishes two definitions of Z_{eff} , $Z_{\text{eff}}^{AA,1} = 2.0$ from the population of KS states with non-negative energy, and $Z_{\text{eff}}^{AA,2} = 3.0$ from the population of KS states similar to the free-electron states [85].

The low-density (0.5 g/cm^3) carbon exhibits clear “bound-free” transitions, making fitting the NBE spectrum to a Drude model a difficult task. We fit the group conductivity to the modified Drude-Lorentz model and extract a $Z_{\text{eff}} = 0.55$; compared to **Tartarus** which produces $Z_{\text{eff}}^{AA,1} = 0.59$ and $Z_{\text{eff}}^{AA,2} = 0.74$. The remainder of the spectral weight is in a Lorentz peak at $\omega_1 = 11.6 \text{ eV}$, proportional to the number of bound electrons. On the other hand, solid-density carbon has a nearly featureless Drude-like conductivity and NBE spectrum. Looking at $\tilde{Z}^*(\omega)$, one may expect that the system characteristics follow a Drude behavior over a large frequency range, yielding $Z_{\text{eff}} \sim 4$. However, a fit to $\sigma^G(\omega)$ reveals a distinct Lorentz peak centered at $\omega_1 = 16.5 \text{ eV}$. This leads to a $Z_{\text{eff}} = 3.1$, while **Tartarus** produces $Z_{\text{eff}}^{AA,1} = 1.47$ and $Z_{\text{eff}}^{AA,2} = 3.45$. The distribution of $\tilde{Z}^*(\omega)$ is significantly larger for the high-density carbon compared to the low-density, as evidenced by the purple and red gradient-shaded lines respectively, in Fig. 2. In all cases the modified Drude-Lorentz model, and the Drude only contribution proportional to Z_{eff} , based on fitting the group conductivity’s, are plotted alongside the calculated results for both $\tilde{Z}^*(\omega)$ and $\sigma^{FD}(\omega)$.

Thus-far we have only considered the group conductivity containing all atoms, which is identical to the regular conductivity. Now we consider the novel case where

we can extract more detailed information by averaging only over subsets of atoms. Specifically we will examine the group conductivity containing atoms of different element types. We present a single warm dense mixture of equal parts hydrogen, beryllium and carbon, elements integral to inertial confinement fusion ablaters and recent experiments [86, 87], at a density of 1.37 g/cm^3 and $k_B T = 5 \text{ eV}$. This system comprises a large simulation box with 128 atoms of each element and high temperature at a relatively low density; physical conditions that challenge the deterministic Kohn-Sham approach [73, 74]. Hence we employ a recently developed mixed stochastic-deterministic TD-DFT to converge the simulation [52, 73]. The force response of each ion (inset) and their element-wise and all-ion averages are shown in Fig. 3(a). As expected, the average force for all ions nearly exactly opposes the time-derivative of the current density per atom (from Eq. (4)). Due to the explicit treatment of Be-1s electrons in the pseudopotential, the Be response features long-lived oscillations which quickly average to zero, but individually persist. In Fig. 3(b), the NBE’s for ions of each species are shown along with $\tilde{Z}(\omega)$ and $\tilde{Z}^{CD}(\omega)$. Figure 3(c) shows the group conductivity for each element type, the sum of the contributions, σ^{FD} , and the regular conductivity σ . The peak in the conductivity starting at $\hbar\omega \sim 100 \text{ eV}$ is solely attributed to Be $1s \rightarrow$ continuum transitions, though it overlaps with the tail of the carbon contribution. A modified Drude-Lorentz fit of each $\sigma^G(\omega)$ yields $\tilde{Z}_{\text{eff}}^{C/H/Be} = 2.36/0.57/1.13$. The NBE calculations indicate charge transfer occurring between the groups, with $\Delta Z_{CT}^{C/H/Be} = +1.05/-0.16/-0.83$ electrons, which follows from the electronegativity of each species. Using a chemical potential matching procedure [42], **Tartarus** produces $Z_{\text{eff}}^{AA,1,C/H/Be} = 2.78/1.0/2.0$ and $Z_{\text{eff}}^{AA,2,C/H/Be} = 1.05/0.45/1.26$.

We present a new formalism for a more efficient cal-

culuation of the $Z_a^*(\omega)$ for all atoms in a unit cell from TDDFT simulations. *Ab initio* calculations of $Z_a^*(\omega)$ could help develop a more complete understanding of the initial nonequilibrium ion-velocity distribution resulting from pulsed-laser excitations in the extreme ultraviolet and soft X-ray regimes. Transforming $Z_a^*(\omega)$ to the force-derived conductivity, $\sigma^{FD}(\omega)$, provides a logical interpretation of the high frequency and imaginary parts of $Z_a^*(\omega)$ and the potential to partition the optical response into atomic groups, *e.g.*, by element types. Our simulations also provide the first numerical validation of the DCS sum rule beyond the static limit. In the warm dense matter regime described here, averaging $Z_a^*(\omega)$ over a sufficiently large number of atoms allows determination of Z_{eff}^G for a subgroup of (or all) atoms. These results tend to fall between the disparate definitions from an average atom code [42]. When applied to the mixed C/H/Be system, we see a charge transfer between the element groups, which unveils a new complexity to the electronic structure of warm dense matter mixtures. This could play a significant role in the mixing of equation-of-state or conductivity tables and model development. Moreover, during the generation of mixed conductivity spectra, the weighted contributions of different species could be compared against the group conductivities, $\sigma^G(\omega)$, generated by our proposed approach.

The calculations in this letter are based on TD-DFT using approximate adiabatic exchange-correlation functionals [88]. More research into the dynamical exchange-correlation effects, and development of acceler-

ated nonequilibrium time-domain methods [89, 90], and their effect on NBEC is warranted. Since the NBEC and group conductivities are well-defined observables, they can in principle be calculated using any excited-state electronic structure approach. However, the extraction of Z_{eff}^G from the NBEC is based on a further assumption, *i.e.*, the Drude-Lorentz picture, and is therefore not a unique estimation of the charge. We have shown that, at least, the NBEC model consistently relates Z_{eff}^G to both the average ionic forces and the nearly-free electron conduction.

ACKNOWLEDGMENTS

This work was supported by the U.S. Department of Energy through the Los Alamos National Laboratory (LANL). Research presented in this article was supported by the Laboratory Directed Research and Development program, projects number 20230322ER and 20230323ER, and the Institute for Material Science, projects number 20248109CT-IMS, of LANL. We acknowledge the support of the Center for Nonlinear Studies (CNLS). This research used computing resources provided by the LANL Institutional Computing and Advanced Scientific Computing programs. Los Alamos National Laboratory is operated by Triad National Security, LLC, for the National Nuclear Security Administration of U.S. Department of Energy (Contract No. 89233218CNA000001).

-
- [1] M. Bonitz, T. Dornheim, Z. A. Moldabekov, S. Zhang, P. Hamann, H. Kählert, A. Filinov, *et al.*, Ab initio simulation of warm dense matter, *Physics of Plasmas* **27**, 042710 (2020).
 - [2] T. Dornheim, Z. A. Moldabekov, K. Ramakrishna, P. Tolias, A. D. Baczewski, D. Kraus, T. R. Preston, *et al.*, Electronic density response of warm dense matter, *Physics of Plasmas* **30**, 032705 (2023).
 - [3] K. Falk, Experimental methods for warm dense matter research, *High Power Laser Science and Engineering* **6**, e59 (2018).
 - [4] W. Lorenzen, A. Becker, and R. Redmer, Progress in warm dense matter and planetary physics, in *Frontiers and Challenges in Warm Dense Matter*, edited by F. Graziani, M. P. Desjarlais, R. Redmer, and S. B. Trickey (Springer International Publishing, Cham, 2014) pp. 203–234.
 - [5] V. B. Prakapenka, N. Holtgrewe, S. S. Lobanov, and A. F. Goncharov, Structure and properties of two superionic ice phases, *Nature Physics* **17**, 1233 (2021).
 - [6] D. e. a. Ehrenreich, Nightside condensation of iron in an ultrahot giant exoplanet, *Nature* **580**, 597 (2020).
 - [7] H. e. a. Abu-Shawareb (The Indirect Drive ICF Collaboration), Achievement of Target Gain Larger than Unity in an Inertial Fusion Experiment, *Phys. Rev. Lett.* **132**, 065102 (2024).
 - [8] M. S. Murillo, J. Weisheit, S. B. Hansen, and M. W. C. Dharma-Wardana, Partial ionization in dense plasmas: Comparisons among average-atom density functional models, *Phys. Rev. E* **87**, 063113 (2013).
 - [9] P. Grabowski, S. Hansen, M. Murillo, L. Stanton, F. Graziani, A. Zylstra, S. Baalrud, *et al.*, Review of the first charged-particle transport coefficient comparison workshop, *High Energy Density Physics* **37**, 100905 (2020).
 - [10] L. J. Stanek, A. Kononov, S. B. Hansen, B. M. Haines, S. X. Hu, P. F. Knapp, M. S. Murillo, *et al.*, Review of the second charged-particle transport coefficient code comparison workshop, *Physics of Plasmas* **31**, 052104 (2024).
 - [11] B. M. Haines, Charged particle transport coefficient challenges in high energy density plasmas, *Physics of Plasmas* **31**, 050501 (2024).
 - [12] R. S. Cohen, L. Spitzer, and P. M. Routly, The Electrical Conductivity of an Ionized Gas, *Phys. Rev.* **80**, 230 (1950).
 - [13] Y. T. Lee and R. M. More, An electron conductivity model for dense plasmas, *The Physics of Fluids* **27**, 1273 (1984).
 - [14] D. Munro and S. Weber, Electron thermal conduction in LASNEX 10.2172/95342 (1994).
 - [15] M. Desjarlais, Practical Improvements to the Lee-More Conductivity Near the Metal-Insulator Transition, *Contributions to Plasma Physics* **41**, 267 (2001).
 - [16] F. Perrot and M. W. C. Dharma-Wardana, Electrical

- resistivity of hot dense plasmas, *Phys. Rev. A* **36**, 238 (1987).
- [17] L. Spitzer and R. Härm, Transport Phenomena in a Completely Ionized Gas, *Phys. Rev.* **89**, 977 (1953).
 - [18] E. Nardi, Z. Zinamon, D. Riley, and N. C. Woolsey, X-ray scattering as a dense plasma diagnostic, *Phys. Rev. E* **57**, 4693 (1998).
 - [19] B. Lihua, Z. Jiyan, Z. Xiaoding, Z. Yang, and D. Yongkun, Observations of non-collective x-ray scattering in warm dense carbon plasma, *Physics of Plasmas* **19**, 122709 (2012).
 - [20] D. Kraus, D. A. Chapman, A. L. Kritcher, R. A. Baggott, B. Bachmann, G. W. Collins, S. H. Glenzer, J. A. Hawreliak, D. H. Kalantar, O. L. Landen, T. Ma, S. Le Pape, J. Nilsen, D. C. Swift, P. Neumayer, R. W. Falcone, D. O. Gericke, and T. Döppner, X-ray scattering measurements on imploding ch spheres at the national ignition facility, *Phys. Rev. E* **94**, 011202 (2016).
 - [21] T. Döppner, M. Bethkenhagen, D. Kraus, P. Neumayer, D. A. Chapman, B. Bachmann, R. A. Baggott, *et al.*, Observing the onset of pressure-driven K-shell delocalization, *Nature* **618**, 270 (2023).
 - [22] J. Ren, Z. Deng, W. Qi, B. Chen, B. Ma, X. Wang, S. Yin, *et al.*, Observation of a high degree of stopping for laser-accelerated intense proton beams in dense ionized matter, *Nature Communications* **11**, 5157 (2020).
 - [23] S. Malko, W. Cayzac, V. Ospina-Bohórquez, K. Bhutwala, M. Bailly-Grandvaux, C. McGuffey, R. Fedosejevs, *et al.*, Proton stopping measurements at low velocity in warm dense carbon, *Nature Communications* **13**, 2893 (2022).
 - [24] C.-K. Li and R. D. Petrasso, Charged-particle stopping powers in inertial confinement fusion plasmas, *Phys. Rev. Lett.* **70**, 3059 (1993).
 - [25] G. Maynard and C. Deutsch, Energy loss and straggling of ions with any velocity in dense plasmas at any temperature, *Phys. Rev. A* **26**, 665 (1982).
 - [26] D. Gericke, M. Schlanges, and W. Kraeft, Stopping power of a quantum plasma — T-matrix approximation and dynamical screening, *Physics Letters A* **222**, 241 (1996).
 - [27] L. S. Brown, D. L. Preston, and R. L. Singleton Jr., Charged particle motion in a highly ionized plasma, *Physics Reports* **410**, 237 (2005).
 - [28] C. F. Clauser and N. R. Arista, Stopping power of dense plasmas: The collisional method and limitations of the dielectric formalism, *Phys. Rev. E* **97**, 023202 (2018).
 - [29] D. Casas, M. D. Barriga-Carrasco, and J. Rubio, Evaluation of slowing down of proton and deuteron beams in CH₂, LiH, and Al partially ionized plasmas, *Phys. Rev. E* **88**, 033102 (2013).
 - [30] J. R. Stallcop and K. W. Billman, Analytical formulae for the inverse bremsstrahlung absorption coefficient, *Plasma Physics* **16**, 1187 (1974).
 - [31] D. Turnbull, J. Katz, M. Sherlock, L. Divol, N. R. Shaffer, D. J. Strozzi, A. Colaïtis, D. H. Edgell, R. K. Follett, K. R. McMillen, P. Michel, A. L. Milder, and D. H. Froula, Inverse Bremsstrahlung Absorption, *Phys. Rev. Lett.* **130**, 145103 (2023).
 - [32] D. Turnbull, J. Katz, M. Sherlock, A. L. Milder, M. S. Cho, L. Divol, N. R. Shaffer, *et al.*, Reconciling calculations and measurements of inverse bremsstrahlung absorption, *Physics of Plasmas* **31**, 063304 (2024).
 - [33] W. L. Slattery, G. D. Doolen, and H. E. DeWitt, Improved equation of state for the classical one-component plasma, *Phys. Rev. A* **21**, 2087 (1980).
 - [34] F. J. Rogers, Ionization equilibrium and equation of state in strongly coupled plasmas, *Physics of Plasmas* **7**, 51 (2000).
 - [35] J. Clérouin, P. Arnault, C. Ticknor, J. D. Kress, and L. A. Collins, Unified Concept of Effective One Component Plasma for Hot Dense Plasmas, *Phys. Rev. Lett.* **116**, 115003 (2016).
 - [36] C. Ticknor, J. D. Kress, L. A. Collins, J. Clérouin, P. Arnault, and A. Decoster, Transport properties of an asymmetric mixture in the dense plasma regime, *Phys. Rev. E* **93**, 063208 (2016).
 - [37] A. J. White, L. A. Collins, J. D. Kress, C. Ticknor, J. Clérouin, P. Arnault, and N. Desbiens, Correlation and transport properties for mixtures at constant pressure and temperature, *Phys. Rev. E* **95**, 063202 (2017).
 - [38] J. P. Hansen, G. M. Torrie, and P. Vieillefosse, Statistical mechanics of dense ionized matter. VII. Equation of state and phase separation of ionic mixtures in a uniform background, *Phys. Rev. A* **16**, 2153 (1977).
 - [39] S. Bastea, Viscosity and mutual diffusion in strongly asymmetric binary ionic mixtures, *Phys. Rev. E* **71**, 056405 (2005).
 - [40] E. M. Epperlein and M. G. Haines, Plasma transport coefficients in a magnetic field by direct numerical solution of the Fokker–Planck equation, *The Physics of Fluids* **29**, 1029 (1986).
 - [41] J. Clérouin, P. Arnault, B.-J. Gréa, S. Guisset, M. Vandenboomgaerde, A. J. White, L. A. Collins, J. D. Kress, and C. Ticknor, Static and dynamic properties of multi-ionic plasma mixtures, *Phys. Rev. E* **101**, 033207 (2020).
 - [42] C. Starrett, N. Shaffer, D. Saumon, R. Perriot, T. Nelson, L. Collins, and C. Ticknor, Model for the electrical conductivity in dense plasma mixtures, *High Energy Density Physics* **36**, 100752 (2020).
 - [43] A. J. White, G. T. Craven, V. Sharma, and L. A. Collins, Optical and transport properties of plasma mixtures from ab initio molecular dynamics, *Physics of Plasmas* **31**, 042706 (2024).
 - [44] R. P. Drake, Properties of high-energy-density plasmas, in *High-Energy-Density Physics: Foundation of Inertial Fusion and Experimental Astrophysics* (Springer International Publishing, Cham, 2018) pp. 51–114.
 - [45] S. X. Hu, L. A. Collins, V. N. Goncharov, J. D. Kress, R. L. McCrory, and S. Skupsky, First-principles investigations on ionization and thermal conductivity of polystyrene for inertial confinement fusion applications, *Physics of Plasmas* **23**, 042704 (2016).
 - [46] R. Ying and G. Kalman, Thomas-Fermi model for dense plasmas, *Phys. Rev. A* **40**, 3927 (1989).
 - [47] R. S. Mulliken, Electronic Population Analysis on LCAO–MO Molecular Wave Functions. I, *The Journal of Chemical Physics* **23**, 1833 (1955).
 - [48] R. F. W. Bader, Atoms in molecules, *Accounts of Chemical Research* **18**, 9 (1985).
 - [49] F. L. Hirshfeld, Bonded-atom fragments for describing molecular charge densities, *Theoretica chimica acta* **44**, 129 (1977).
 - [50] K. B. Wiberg and P. R. Rablen, Atomic Charges, *The Journal of Organic Chemistry* **83**, 15463 (2018).
 - [51] C. Ertural, S. Steinberg, and R. Dronskowski, Development of a robust tool to extract mulliken and löwdin charges from plane waves and its application to solid-state materials, *RSC Adv.* **9**, 29821 (2019).

- [52] A. J. White, L. A. Collins, K. Nichols, and S. X. Hu, Mixed stochastic-deterministic time-dependent density functional theory: application to stopping power of warm dense carbon, *Journal of Physics: Condensed Matter* **34**, 174001 (2022).
- [53] M. Bethkenhagen, B. B. L. Witte, M. Schörner, G. Röpke, T. Döppner, D. Kraus, S. H. Glenzer, P. A. Sterne, and R. Redmer, Carbon ionization at gigabar pressures: An ab initio perspective on astrophysical high-density plasmas, *Phys. Rev. Res.* **2**, 023260 (2020).
- [54] S. X. Hu, Continuum Lowering and Fermi-Surface Rising in Strongly Coupled and Degenerate Plasmas, *Phys. Rev. Lett.* **119**, 065001 (2017).
- [55] K. P. Driver, F. Soubiran, and B. Militzer, Path integral Monte Carlo simulations of warm dense aluminum, *Phys. Rev. E* **97**, 063207 (2018).
- [56] P. Ghosez, J.-P. Michenaud, and X. Gonze, Dynamical atomic charges: The case of ABO_3 compounds, *Phys. Rev. B* **58**, 6224 (1998).
- [57] M. Born and K. Huang, *Dynamical Theory of Crystal Lattices* (1998).
- [58] S. Baroni, S. de Gironcoli, A. Dal Corso, and P. Giannozzi, Phonons and related crystal properties from density-functional perturbation theory, *Rev. Mod. Phys.* **73**, 515 (2001).
- [59] P. T. Mahon and J. E. Sipe, Electric polarization and magnetization in metals, *SciPost Phys.* **14**, 058 (2023).
- [60] R. Resta and D. Vanderbilt, Theory of polarization: A modern approach, in *Physics of Ferroelectrics: A Modern Perspective* (Springer Berlin Heidelberg, Berlin, Heidelberg, 2007) pp. 31–68.
- [61] C. E. Dreyer, S. Coh, and M. Stengel, Nonadiabatic Born Effective Charges in Metals and the Drude Weight, *Phys. Rev. Lett.* **128**, 095901 (2022).
- [62] R. M. Pick, M. H. Cohen, and R. M. Martin, Microscopic Theory of Force Constants in the Adiabatic Approximation, *Phys. Rev. B* **1**, 910 (1970).
- [63] G. Bellomia and R. Resta, Drude weight in systems with open boundary conditions, *Phys. Rev. B* **102**, 205123 (2020).
- [64] R. Resta, Drude weight and superconducting weight, *Journal of Physics: Condensed Matter* **30**, 414001 (2018).
- [65] R. More, Pressure Ionization, Resonances, and the Continuity of Bound and Free States (Academic Press, 1985) pp. 305–356.
- [66] J. Daligault and J. Simoni, Theory of the electron-ion temperature relaxation rate spanning the hot solid metals and plasma phases, *Phys. Rev. E* **100**, 043201 (2019).
- [67] G. Marchese, F. Macheda, L. Binci, M. Calandra, P. Barone, and F. Mauri, Born effective charges and vibrational spectra in superconducting and bad conducting metals, *Nature Physics* **20**, 88 (2024).
- [68] L. Binci, P. Barone, and F. Mauri, First-principles theory of infrared vibrational spectroscopy of metals and semimetals: Application to graphite, *Phys. Rev. B* **103**, 134304 (2021).
- [69] Andrade, Xavier, Hamel, Sébastien, and Correa, Alfredo A., Negative differential conductivity in liquid aluminum from real-time quantum simulations, *Eur. Phys. J. B* **91**, 229 (2018).
- [70] A. Kononov, C.-W. Lee, T. P. dos Santos, B. Robinson, Y. Yao, Y. Yao, X. Andrade, A. D. Baczewski, E. Constantinescu, A. A. Correa, Y. Kanai, N. Modine, and A. Schleife, Electron dynamics in extended systems within real-time time-dependent density-functional theory, *MRS Communications* **12**, 1002 (2022).
- [71] A. Kononov, A. J. White, K. A. Nichols, S. X. Hu, and A. D. Baczewski, Reproducibility of real-time time-dependent density functional theory calculations of electronic stopping power in warm dense matter, *Physics of Plasmas* **31**, 043904 (2024).
- [72] N. D. Mermin, Thermal Properties of the Inhomogeneous Electron Gas, *Phys. Rev.* **137**, A1441 (1965).
- [73] A. J. White and L. A. Collins, Fast and Universal Kohn-Sham Density Functional Theory Algorithm for Warm Dense Matter to Hot Dense Plasma, *Phys. Rev. Lett.* **125**, 055002 (2020).
- [74] V. Sharma, L. A. Collins, and A. J. White, Stochastic and mixed density functional theory within the projector augmented wave formalism for simulation of warm dense matter, *Phys. Rev. E* **108**, L023201 (2023).
- [75] C.-Y. Wang, S. Sharma, E. K. U. Gross, and J. K. Dewhurst, Dynamical Born effective charges, *Phys. Rev. B* **106**, L180303 (2022).
- [76] T. J. Park and J. C. Light, Unitary quantum time evolution by iterative Lanczos reduction, *The Journal of Chemical Physics* **85**, 5870 (1986).
- [77] S. Goedecker, M. Teter, and J. Hutter, Separable dual-space Gaussian pseudopotentials, *Phys. Rev. B* **54**, 1703 (1996).
- [78] D. R. Hamann, Optimized norm-conserving Vanderbilt pseudopotentials, *Phys. Rev. B* **88**, 085117 (2013).
- [79] M. van Setten, M. Giantomassi, E. Bousquet, M. Verstraete, D. Hamann, X. Gonze, and G.-M. Rignanese, The PseudoDojo: Training and grading a 85 element optimized norm-conserving pseudopotential table, *Computer Physics Communications* **226**, 39 (2018).
- [80] P. Minary, G. J. Martyna, and M. E. Tuckerman, Algorithms and novel applications based on the isokinetic ensemble. II. Ab initio molecular dynamics, *J. Chem. Phys.* **118**, 2527 (2003).
- [81] H. J. Monkhorst and J. D. Pack, Special points for Brillouin-zone integrations, *Phys. Rev. B* **13**, 5188 (1976).
- [82] E. Runge and E. K. U. Gross, Density-Functional Theory for Time-Dependent Systems, *Phys. Rev. Lett.* **52**, 997 (1984).
- [83] D. E. Kelleher and L. I. Podobedova, Atomic transition probabilities of aluminum. a critical compilation, *Journal of Physical and Chemical Reference Data* **37**, 709 (2008).
- [84] N. Gill and C. Starrett, Tartarus: A relativistic Green's function quantum average atom code, *High Energy Density Physics* **24**, 33 (2017).
- [85] C. Starrett, N. Gill, T. Sjostrom, and C. Greeff, Wide ranging equation of state with Tartarus: A hybrid Green's function/orbital based average atom code, *Computer Physics Communications* **235**, 50 (2019).
- [86] O. A. Hurricane, P. K. Patel, R. Betti, D. H. Froula, S. P. Regan, S. A. Slutz, M. R. Gomez, and M. A. Sweeney, Physics principles of inertial confinement fusion and U.S. program overview, *Rev. Mod. Phys.* **95**, 025005 (2023).
- [87] S. Jiang, O. L. Landen, H. D. Whitley, S. Hamel, R. London, D. S. Clark, P. Sterne, S. B. Hansen, S. X. Hu, G. W. Collins, and Y. Ping, Thermal transport in warm dense matter revealed by refraction-enhanced x-ray radiography with a deep-neural-network analysis, *Communications Physics* **6**, 98 (2023).
- [88] L. Lacombe and N. T. Maitra, Non-adiabatic approx-

imations in time-dependent density functional theory: progress and prospects, [npj Computational Materials](#) **9**, 124 (2023).

- [89] M. Bonitz, J.-P. Joost, C. Makait, E. Schroedter, T. Kalsberger, and K. Balzer, Accelerating Nonequilibrium Green Functions Simulations: The G1–G2 Scheme and Beyond, [physica status solidi \(b\)](#) **261**, 2300578 (2024).
- [90] T. Dornheim, Z. A. Moldabekov, K. Ramakrishna, P. Tolias, A. D. Baczewski, D. Kraus, T. R. Preston, D. A. Chapman, M. P. Böhme, T. Döppner, F. Graziani, M. Bonitz, A. Cangi, and J. Vorberger, Electronic density response of warm dense matter, [Physics of Plasmas](#) **30**, 032705 (2023).

Supplemental Material for

Group Conductivity and Dynamical Born Effective Charges of Disordered Metals,
Warm Dense Matter and Dense Plasma Mixtures

Vidushi Sharma^{1,2,3} and Alexander J. White¹

¹*Theoretical Division, Los Alamos National Laboratory, Los Alamos, NM 87545, USA*

²*Center for Nonlinear Studies (CNLS), Los Alamos National Laboratory, Los Alamos, NM 87545, USA*

³*Applied Materials and Sustainability Sciences, Princeton Plasma Physics Laboratory, Princeton, NJ 08540-6655, USA*

(Dated: February 27, 2025)

S1. TIME-DEPENDENT KOHN-SHAM APPROACH TO LINEAR RESPONSE CONDUCTIVITY AND NONADIABATIC BORN EFFECTIVE CHARGE

Since conductivity and NBEC are quantum mechanical observables with well-defined operators, they can be calculated using any time-dependent or excited-state electronic structure method. Here we calculate and analyze the NBEC and group conductivity for bulk systems using time-dependent Kohn-Sham density functional theory (TD-DFT). TD-DFT is the current state of the art excited-state method for large systems with hundreds to thousands of atoms and for warm dense matter, where high temperatures lead to an additional increase in computational cost. Calculations including dynamic correlation, such as, GW and time-dependent Bethe-Salpeter, may improve the results but are beyond the scope of this letter. We utilize atomic units such that the mass of electron, m_e , and the reduced Planck's constant \hbar are unity. Within linear response, the time-dependent NBEC tensor is defined as the response function of the negative of the atomic force vector with respect to the electric field vector,

$$d\mathbf{F}^a(t, \mathbf{q}) \equiv - \int \int dt' d\mathbf{q}' \hat{Z}_a^*(t, t', \mathbf{q}, \mathbf{q}') \cdot d\mathbf{E}(\mathbf{q}', t'), \quad (\text{S1})$$

while the conductivity tensor is defined by a similar equation with the negative of the force replaced by the current density,

$$d\mathbf{J}(t, \mathbf{q}) \equiv \int \int dt' d\mathbf{q}' \hat{\sigma}(t, t', \mathbf{q}, \mathbf{q}') \cdot d\mathbf{E}(\mathbf{q}', t'). \quad (\text{S2})$$

Here \mathbf{q} is the perturbation wavevector. If we consider a macroscopic instantaneous electric field pulse along an arbitrarily chosen x -direction, $dE_x(q', t') = E_0 \delta(q') \delta(t')$, we can obtain the macroscopic NBEC / conductivity via

$$\hat{Z}_{a,y,x}^*(\omega) \equiv \mathcal{F}[\Theta(t) dF^{a,y}(t)/E_0](\omega), \quad (\text{S3})$$

$$\sigma_{y,x}^*(\omega) \equiv \mathcal{F}[\Theta(t) dJ^y(t)/E_0](\omega), \quad (\text{S4})$$

where $\mathcal{F}[\dots]$ denotes the Fourier transform from the forward time t to angular-frequency ω ; the Heaviside function, $\Theta(t)$ is included to ensure causality.

To calculate the time-dependent forces and current from ‘adiabatic’ TD-DFT we solve the equation of motion for the KS Bloch orbitals:

$$\frac{i\partial}{\partial t} u_b^{\mathbf{k}}(\mathbf{r}, t) = \hat{H}_{KS}^{\mathbf{k}}(t) u_b^{\mathbf{k}}(t), \quad (\text{S5})$$

$$\hat{H}_{KS}^{\mathbf{k}}(t) = -\frac{1}{2}(\hat{\nabla} + i\mathbf{A}(t) + i\mathbf{k})^2 + V_{XC,H}(\mathbf{r}, \rho(t)) + V_{ei,LPP}(\mathbf{r}, \mathbf{R}) + \hat{V}_{ei,NLPP}^{\mathbf{k}}(\mathbf{R}). \quad (\text{S6})$$

Here the term ‘adiabatic’ refers to the dependence of the exchange-correlation (plus Hartree) potential, $\hat{V}_{XC,H}$, on only the instantaneous time-dependent density, $\rho(t)$; \mathbf{r} is the real-space electron position vector while \mathbf{R} is the ion position vector, \mathbf{k} is the k-point associated with this Bloch orbital. When using pseudopotentials (PP), the electron-ion interaction has a local part, $V_{ei,LPP}(\mathbf{r}, \mathbf{R})$, and possibly a nonlocal part, $\hat{V}_{ei,NLPP}^{\mathbf{k}}(\mathbf{R})$. The time-dependent density (density matrix) is given by:

$$\rho(\mathbf{r}, t) = \delta(\mathbf{r}, \mathbf{r}') \rho(\mathbf{r}, \mathbf{r}', t) = \delta(\mathbf{r}, \mathbf{r}') \sum_{\mathbf{k}, b} f(\varepsilon_b^{\mathbf{k}}, \mu, T) u_b^{\mathbf{k}}(\mathbf{r}, t) u_b^{*\mathbf{k}}(\mathbf{r}', t), \quad \text{where} \quad (\text{S7})$$

$$f(\varepsilon, \mu, T) := \frac{1}{1 + e^{(\varepsilon - \mu)/k_B T}}. \quad (\text{S8})$$

In Mermin's extension of TD-DFT, the finite electron temperature [72] T , enters only through the Fermi-Dirac occupations, which depend on the equilibrium Mermin-DFT eigenenergies, ε , and the electron chemical potential, μ . For mixed stochastic-deterministic KS-DFT, the density matrix contains also the complementary stochastic vectors, which take a similar low-rank form to Eq. (S7), and it is propagated by the same TD approach as the deterministic orbitals [52, 73, 74].

For our instantaneous electric field pulse along x , the vector potential is a step function, $\mathbf{A}(t) \equiv -\hat{e}_x E_0 \Theta(t)$. Recall that $\mathbf{E}(t) = -\frac{\partial}{\partial t} \mathbf{A}(t)$. The electron momentum is thus instantaneously increased and relaxes due to disorder. From the Mermin-DFT approach, the initial current density before the pulse is zero, $J(t < 0) = 0$.

The force is calculated using the energy-conserving Ehrenfest expression:

$$F^{a,y}(f) = \int d\mathbf{r} \left[\left\{ \frac{\partial}{\partial R_{a,y}} V_{ei,\text{LPP}}(\mathbf{r}, \mathbf{R}) \right\} \rho(\mathbf{r}, t) \right] + \sum_{b,\mathbf{k}} \int \int d\mathbf{r} d\mathbf{r}' f(\varepsilon_b^{\mathbf{k}}, \mu, T) u_b^{\mathbf{k}*}(\mathbf{r}', t) \left\{ \frac{\partial}{\partial R_{a,y}} V_{ei,\text{NLPP}}(\mathbf{r}, \mathbf{r}', \mathbf{R}) \right\} u_b^{\mathbf{k}}(\mathbf{r}, t) . \quad (\text{S9})$$

The total electron current can be decomposed into the diamagnetic part, a contribution coming directly from electron density $\rho(r)$ and vector potential, and the paramagnetic part, coming from the time-dependent density matrix, $\hat{\rho}(t)$,

$$\mathbf{J}(t) = \int d\mathbf{r} \mathbf{A}(r, t) \rho(r) + \text{Tr} [\{\hat{\mathbf{p}}\} \hat{\rho}(t)] , \quad (\text{S10})$$

where $\mathbf{p} = (-i\nabla + \mathbf{k})$ is the canonical electron momentum. Non-local Hamiltonian terms, such as arising from pseudopotentials, add additional terms to the “full” momentum, as defined via $\mathbf{p}' = i[\hat{H}_{KS}^{\mathbf{k}}, \mathbf{r}]$. This “full” definition retains consistency of the dipole and the momentum operators, while the first fulfils the exact momentum conservation and thus the generalized Dreyer, Coh, and Stengel (DCS) rule as well as the f-sum rule [61, 64]. We employ the canonical momentum in the letter and note that differences are typically less than ~ 10 per cent.

For simplicity, we only discuss response parallel to the direction of perturbation, dropping vector and tensor notation, and only concern ourselves with the macroscopic ($q \rightarrow 0$) limit. We consider only isotropic systems in the letter and thus, do not investigate the off-diagonal elements of the NBEC or conductivity tensors.

S2. CURRENT RESPONSE TO MACROSCOPIC ELECTRIC FIELD PULSE AND THE DRUDE WEIGHT

The conductivity can be separated into two parts, the regular and Drude contributions, [63, 64]

$$\sigma(\omega) = \frac{D}{\pi} \left\{ \frac{1}{2} \delta(\omega) + \frac{i}{\omega} \right\} + \sigma_{\text{reg}}(\omega) . \quad (\text{S11})$$

The Drude part, $\propto D/\pi$, and regular conductivity, σ_{reg} , are associated with intraband and interband transitions, respectively. Finite D implies the presence of free charge carriers, *i.e.*, a finite long-time current density $\mathbf{J}(t \rightarrow \infty) \neq 0$ in response to an instantaneous macroscopic electric field pulse at $t = 0$. The electric field imparts momentum to all the electrons equally, but some electrons have high inertia and thus there is a finite current at long times, *i.e.*, timescales of the order of ion motion or phonon frequencies. Finite simulation time and system size necessitate a dampening of the current before the Fourier transformation, leading to a broadening of the conductivity peaks and a finite regular conductivity at $\omega = 0$. By causality, the imaginary part of the conductivity, $\Im[\sigma(\omega)]$, is an odd function, so the real part of the $\Re[i\omega \sigma(\omega)]|_{\omega=0} = 0$, therefore from

$$i\omega \hat{\sigma}(\omega) \equiv -\frac{\hat{D}}{\pi} + i\omega \hat{\sigma}_{\text{reg}}(\omega) , \quad \text{and} \quad (\text{S12})$$

$$i\omega \hat{\sigma}_{\text{reg}}(\omega) = \frac{\mathbf{J}(0^+)}{\mathbf{E}_0} + \frac{1}{\mathbf{E}_0} \mathcal{F} \left[\Theta(t) e^{-\frac{1}{4}\gamma^2 t^2} \frac{\partial}{\partial t} \mathbf{J}(t, \mathbf{q} = 0) \right] (\omega) , \quad (\text{S13})$$

we can extract the Drude weight, $\hat{D}/\pi = \Re[i\omega \hat{\sigma}_{\text{reg}}(\omega)]|_{\omega=0}$, directly from the current in the presence of a broadened ($\gamma > 0$) regular conductivity. To have the correct $\omega \rightarrow \infty$ behavior in $i\omega \hat{\sigma}(\omega)$, the dampening term is included after taking the time-derivative. Since electrons cannot respond instantaneously to the pulse, the current at a time instant infinitesimally after the pulse is proportional to the electric field strength and the electron density, $\mathbf{J}(0^+) = n_e \mathbf{E}_0$, which implies, $\int \frac{d\omega}{2\pi} \sigma(\omega) = \frac{n_e}{2}$. [64] This is the well-known f-sum rule. More simply put, the Drude weight is proportional to the initial current density plus the (negative) change in the current density over a long time, *i.e.*, it is the *unrelaxed* part of the current density.

S3. VALIDATION OF APPROACH AGAINST SYSTEMS SIMULATED IN “DYNAMICAL BORN EFFECTIVE CHARGES” BY C.-YU WANG, S. SHARMA, E. K. U. GROSS, AND J. K. DEWHURST [75]

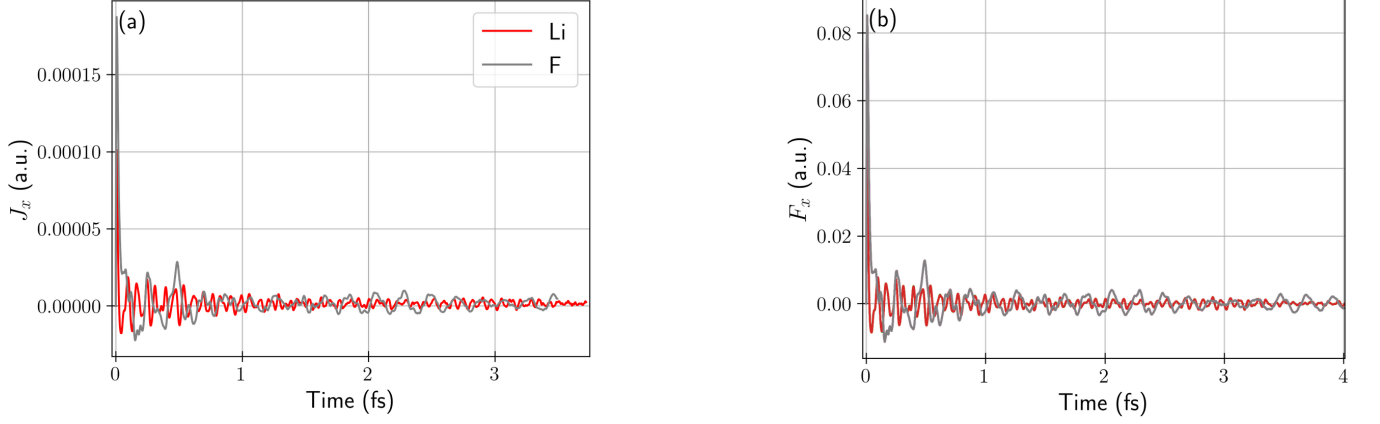


FIG. S1. LiF fcc crystal structure with an 8-atom unit cell and a $[20 \times 20 \times 20]$ Monkhorst-pack k -grid: (a) Current density signal decay with time for an initial perturbation given by an atomic displacement $\lambda(t = 0^-) : \delta r = 0.01$ a.u., in the x -direction. (b) Forces exerted on the atoms by the electronic density in response to an electric field pulse uniform in space in the long-wavelength limit $\lambda(t = 0^-) : E_x = 0.01$ a.u.

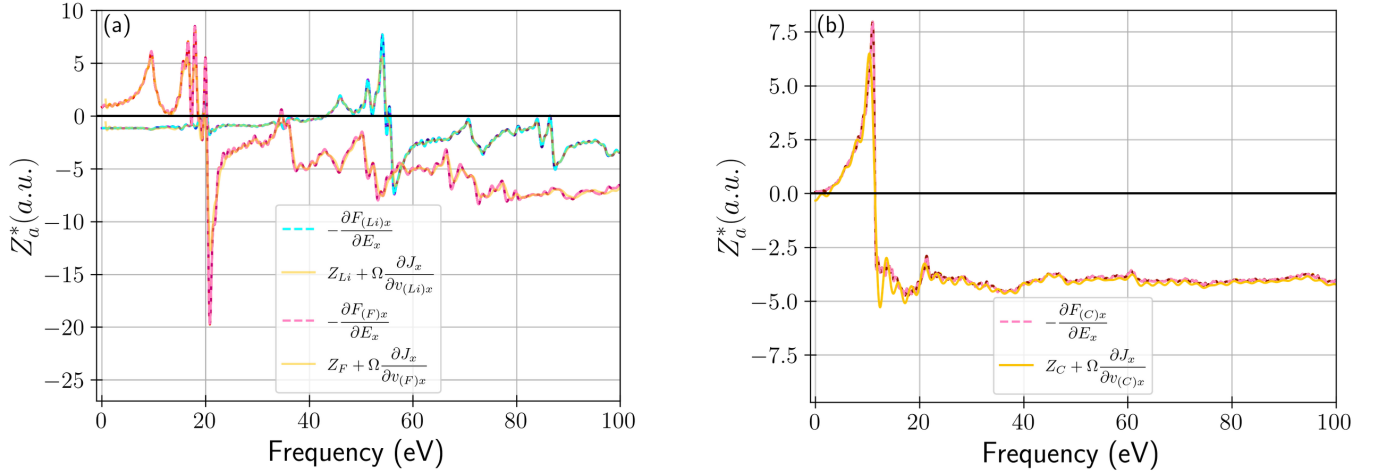


FIG. S2. Nonadiabatic Born Effective Charges Z_a^* : (a) 8-atom unit cell of LiF fcc crystal, and (b) 8-atom unit cell of C diamond, computed using two equivalent definitions of perturbation-response measures.

A real-time TDDFT-based dynamics, assuming fixed nuclear positions, of the system after an initial perturbation, λ , reveals the relaxation of the electronic system and the subsequent measure of Born effective charge tensor, Z_{ij}^* . A Gaussian smearing γ is used for Fourier transforming the signal to the frequency domain, *vide infra* for values. In Ref. [75] the authors use an instantaneous atomic displacement as the initial perturbation and calculated the time-dependent current response. This is based on the relationship:

$$\hat{Z}_a^* = Z_a \hat{I} + \frac{\partial \mathbf{P}}{\partial \mathbf{R}^a} \equiv Z_a \hat{I} + \frac{\partial \mathbf{J}}{\partial \mathbf{v}^a}, \quad \text{with} \quad (S14)$$

$$\lambda(t) \equiv \delta \mathbf{R}^a \Theta(t - t_0) = \int_{-\infty}^t dt' \mathbf{v}^a(t'), \quad \text{where } \mathbf{v}^a(t') \equiv \delta \mathbf{R}^a \delta(t' - t_0),$$

where \mathbf{v}^a is the velocity of the ion, a . Θ is the Heaviside function. We propose the calculations based on the

instantaneous macroscopic electric field pulse:

$$\begin{aligned} \hat{Z}_a^* &= -\frac{\partial \mathbf{F}_a}{\partial \mathbf{E}}, \quad \text{with} \\ \lambda(t) &\equiv \delta \mathbf{A} \Theta(t - t_0) = \int_{-\infty}^t dt' \mathbf{E}(t'), \quad \text{where } \mathbf{E}(t') \equiv \delta \mathbf{A} \delta(t' - t_0). \end{aligned} \quad (\text{S15})$$

This has the same advantage for calculation of nonadiabatic BEC as it does for the static BEC, the time-dependent propagation (or self-consistent DFPT) can be done for one perturbation, while calculating the observable many times. We validate our approach by comparing with certain calculations carried out in Ref. [75], namely ambient conditions lithium fluoride, and diamond, along with aluminium already included in the main text. This also allows us to compare the effect of using semi-core and frozen core pseudopotentials against the all-electron calculations in Ref. [75]. We calculate similar spectra compared to Ref. [75], with large deviations occurring only at large frequencies, where the effect of the pseudopotentials becomes prominent. We see excellent agreement between the two approaches for calculating $\hat{Z}_a^*(\omega)$, in both time (Fig. S1) and frequency domains (Fig. S2).

S4. MODIFIED DRUDE-LORENTZ MODEL FOR FITTING GROUP CONDUCTIVITY AND NONADIABATIC BORN EFFECTIVE CHARGE

$$\begin{aligned} \sigma_{MDL}([Z_{val}, \Delta Z_{CT}, n], \{Z_{eff}, \tau_0, \omega_1, \tau_1, \}, \omega) &= \frac{\{Z_{eff} + \Delta Z_{CT}\} n \tau_0}{1 - i\omega \tau_0} + \frac{\{Z_{val} - Z_{eff}\} n \omega \tau_1}{\omega + i(\omega_1^2 - \omega^2) \tau_1}, \\ \sigma_{MDL}^G(\omega) &\equiv \Re\{\sigma_{MDL}([Z_{val}^G, \Delta Z_{CT}^G, n^G], \{Z_{eff}^G, \tau_0^G, \omega_1^G, \tau_1^G\}, \omega)\}, \\ \bar{Z}_{G,MDL}^*(\omega) &\equiv -\Im\{\omega \times \sigma_{MDL}([Z_{val}^G, \Delta Z_{CT}^G, n^G], \{Z_{eff}^G, \tau_0^G, \omega_1^G, \tau_1^G\}, \omega)\} + \Delta Z_{CT}^G. \end{aligned} \quad (\text{S16})$$

Here τ_0 and τ_1 are the scattering times for the group's free and bound electrons; ω_1 is the frequency of the bound electrons modeled as a Lorentz oscillator; and Z_{eff} is the free electron number (the average ionization) excluding the number of charge-transferred electrons ΔZ_{CT} . This maintains the convention that $Z_{val} = Z_{eff} + Z_{bound}$, where Z_{val} is the number of valence electrons that are tightly bound to the nuclei. Parameters $[Z_{val}, \Delta Z_{CT}, n]$ are constrained, with $\Delta Z_{CT}^G \equiv \bar{Z}_G^*(0)$, and n^G is the number density for the group atoms. Parameters $\{Z_{eff}, \tau_0, \omega_1, \tau_1, \}$ are the model fit parameters, such that no parameter is negative and Z_{eff} is upper-bound by Z_{val} . When the NBECs are partitioned into groups, the individual $\bar{Z}_G^*(\omega)$ can be finite at zero frequency, even when $D = 0$, due to charge transfer between the partitions. This was shown previously in insulating lithium hydride and boronitride.[75] In disordered conducting systems the transferred electrons, ΔZ_{CT}^G , may contribute to the conductivity as “nearly-free” electrons ascribed to a particular group, raising the effective charge. But this charge transfer does not affect the high frequency limit of the NBEC, $Z_a^*(\infty) = Z_{a,val}$, which only depends on Z_{val} . Our modified Drude-Lorentz plus charge transfer model, Eq. (S16) accounts for this.

TABLE S1. Table of fit parameters for the modified Drude-Lorentz model used to extract Z_{eff}^G .

Group	ρ [g/cm ³]	$k_B T$ [eV]	Z_{eff}	τ_0 (fs)	$Z_{val} - Z_{eff}$	ω_1 (eV)	τ_1 (fs)
Al	2.7	1.0	3.0	0.48	0.0	—	—
C	0.5	1.0	0.55	0.08	3.45	11.6	0.05
C	3.52	1.0	3.1	0.05	0.9	16.5	0.04
All atoms C-Be-H	1.37	5.0	1.40	0.072	0.93	10.4	0.04
C in C-Be-H	—	—	2.36	0.067	1.64	11.1	0.03
Be in C-Be-H	—	—	1.14	0.14	0.86	8.8	0.05
H in C-Be-H	—	—	0.57	0.085	0.43	9.3	0.05

For the carbon results the valence includes the four $2s, 2p$ electrons which is also the number of electrons treated explicitly in the TD-DFT calculations. For the beryllium results the valence includes only the $2s$ electrons while the $1s$ electrons are also explicitly treated in the TD-DFT calculation. The response of the $1s$ electrons only occurs at $\omega > 100$ eV, and we can safely assume the $1s$ electrons are not ionized for frequencies below this. The fit of the group conductivity for the C-Be-H system ranges from 0 – 75 eV, to avoid the Be $1s$ excitations.

The fit of the total force-derived conductivity $\sigma^{FD}(\omega) = \{\sigma^C(\omega) + \sigma^{Be}(\omega) + \sigma^H(\omega)\}$ can be compared to the individual element group fits. If we had perfect “nearly-free” Drude contributions only then we would have $Z_{eff}^{Avg} = \frac{1}{3}\{Z_{eff}^C + Z_{eff}^{Be} + Z_{eff}^H\}$. This is approximately satisfied in our system (1.40 to 1.36). We would also have $\tau_0^{Avg} = \{Z_{eff}^C\tau_0^C + Z_{eff}^{Be}\tau_0^{Be} + Z_{eff}^H\tau_0^H\} / \{Z_{eff}^C + Z_{eff}^{Be} + Z_{eff}^H\}$. Our fit results in $\tau_1^{avg} = 0.072$ fs compared to 0.088 fs. Overlap of the Lorentz oscillators with the Drude contribution, as well as limitations of the fitting model to one oscillator, lead to the differences.

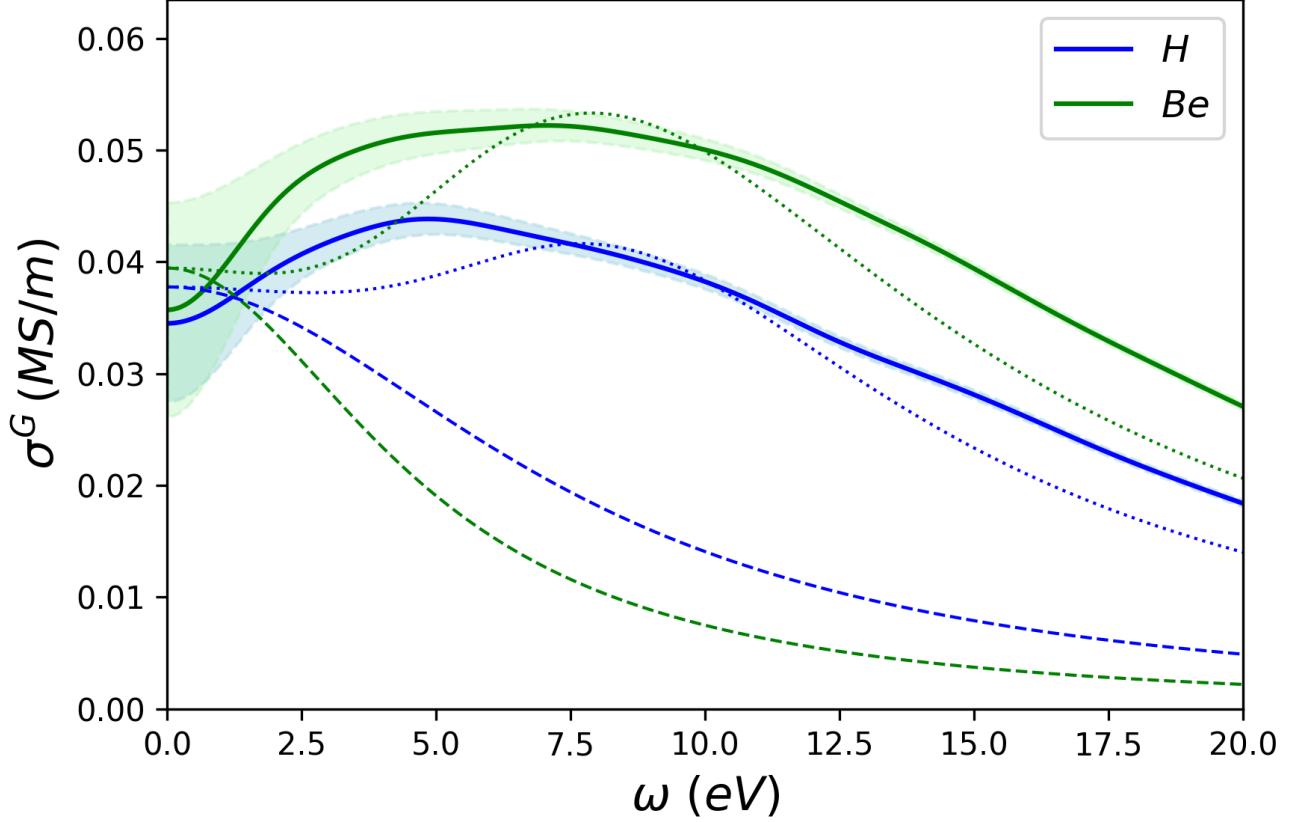


FIG. S3. Fitting of C/H/Be mixture (1.37 g/cm³, 5 eV) elemental group conductivities, for H and Be, to the modified Drude-Lorentz model. Solid-Line is the group conductivity, colored band ranges from ± 1 standard error. Dotted line is modified Drude-Lorentz model fit, dashed line is the Drude only portion (proportional to Z_{eff}^G). Low frequency portion is highlighted to show fit and standard error.

S5. SIMULATION DETAILS

All simulations in the letter and these supplemental materials are performed via time-dependent Kohn-Sham density functional theory. We apply either fully deterministic or mixed stochastic-deterministic approaches, using the pseudopotential plane-wave DFT code SHRED (Stochastic and Hybrid Representation of Electronic structure by Density functional theory) developed by the authors at Los Alamos National Laboratory [52, 73]. Table S2 shows the parameters used to perform the simulations. We utilize the Short Iterative Lanczos propagation scheme [76], with no enforced time reversal symmetry. For section S3, we utilize Hartwigsen-Goedecker-Hutter (HGH) pseudopotentials from the cp2k database [77]. For the simulations presented in the letter, we utilize Optimized Norm-Conserving Vanderbilt pseudopotentials [78] (ONCV, version 3.2.3) from the PseudoDojo repository [79]. For Figure 1 of the letter the FCC results are compared to a single disordered ion configuration taken from molecular dynamics simulation. For Figures 2(3), we average over 5(4) ion configurations sampled from molecular dynamics simulations, performed using the SHRED code. To generate the atomic configurations for WDM systems, we carried out Born-Oppenheimer

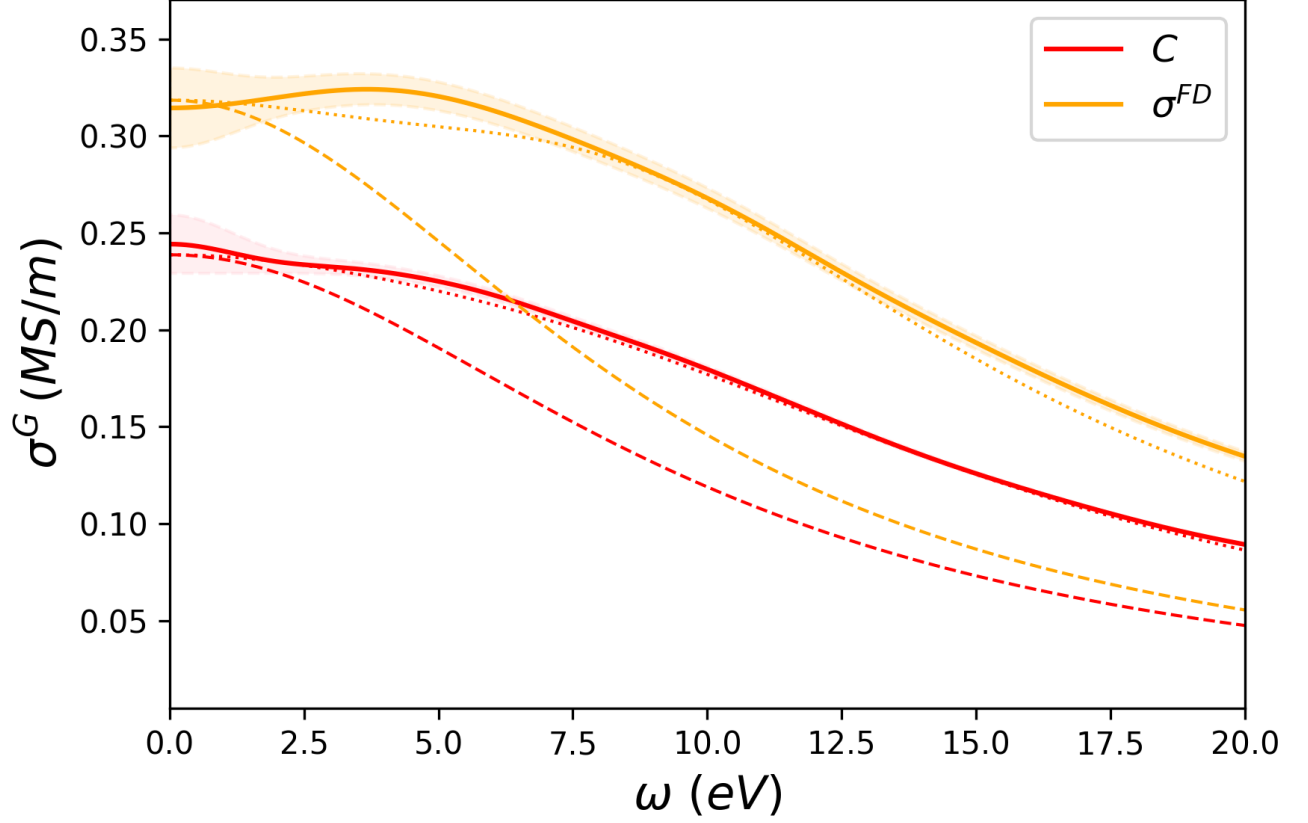


FIG. S4. Fitting of C/H/Be mixture (1.37 g/cm³, 5 eV) elemental group conductivities, for C and the total force-derived conductivity ($\sigma^{FD}(\omega)$), to the modified Drude-Lorentz model. Solid line is the group conductivity, colored band ranges from ± 1 standard error. Dotted line is modified Drude-Lorentz model fit, dashed line is the Drude only portion (proportional to Z_{eff}^G). Low frequency portion is highlighted to show fit and standard error.

molecular dynamics (BOMD) simulations in an isokinetic (canonical NVT)[80]ensemble using a GGA-PBE exchange-correlation functional; the time-step is based on Wigner-Seitz radius and temperature. After an initial equilibration period, each snapshot is sampled from the production BOMD with sufficient period to ensure uncorrelated snapshots. These snapshots were further used as structures for the TD-DFT real-time dynamics.

TABLE S2. Simulation parameters for the letter and supplemental materials. Key: ρ - total mass density, $k_B T$ - electron temperature, N_ψ - number of deterministic Kohn Sham orbitals, N_χ - number of complementary stochastic vectors, k-grid - Broullion Zone sample via Monkhorst-Pack grids (no Γ) [81], N_a - number of atoms in unit cell, Ecut - maximum planewave energy defining basis and real-space grid, γ - the Gaussian dampening coefficient / broadening parameter, E_0 - the perturbing electric field strength, dt the electronic time step.

System	ρ [g/cm ³]	$k_B T$ [eV]	N_ψ	N_χ	k-grid	N_a	Ecut [eV]	γ [eV]	E_0 [a.u.]	dt [a.u.]
-Letter-										
Al (FCC)	2.7	0.025	14	0	$16 \times 16 \times 16$	4	500	0.136	0.01	0.05
Al (FCC)	2.7	1.0	28	0	$16 \times 16 \times 16$	4	500	0.136	0.01	0.05
Al (FCC)	2.7	3.0	42	0	$16 \times 16 \times 16$	4	500	0.136	0.01	0.05
Al (FCC)	2.7	5.0	84	0	$16 \times 16 \times 16$	4	500	0.136	0.01	0.05
Al (WDM)	2.7	1.0	224	0	$2 \times 2 \times 2$	64	500	0.015	0.01	0.05
C (WDM)	0.5	1.0	320	0	Γ -point	64	1000	0.272	0.01	0.022
C (WDM)	3.52	1.0	224	0	$2 \times 2 \times 2$	64	1000	0.272	0.01	0.021
C-Be-H (WDM)	1.37	5.0	1120	112	Γ -point	128/128/128	1200	1.36	0.1	0.018
-Supplemental-										
Li-F (fcc)	2.53	0.025	24	0	$20 \times 20 \times 20$	4/4	500	0.136	0.01	0.043
C (Diamond)	3.53	0.025	16	0	$20 \times 20 \times 20$	4	500	0.136	0.01	0.043